Crossover Interference in *Saccharomyces cerevisiae* Requires a *TID1/RDH54*- and *DMC1*-Dependent Pathway

Miki Shinohara,*[†,1] Kazuko Sakai,[†] Akira Shinohara*[,†,‡] and Douglas K. Bishop*[,2]

**Department of Radiation and Cellular Oncology and Department of Molecular Genetics and Cell Biology, University of Chicago, Chicago, Illinois 60637, [†]Department of Biology, Graduate School of Science, Osaka University, Toyonaka, Osaka 560-0043, Japan and [‡]Precursory Research for Embryonic Science and Technology, Japanese Science and Technology, Toyonaka, Osaka 560-0043, Japan*

Manuscript received October 9, 2002
Accepted for publication January 2, 2003

ABSTRACT

Two RecA-like recombinases, Rad51 and Dmc1, function together during double-strand break (DSB)-mediated meiotic recombination to promote homologous strand invasion in the budding yeast *Saccharomyces cerevisiae*. Two partially redundant proteins, Rad54 and Tid1/Rdh54, act as recombinase accessory factors. Here, tetrad analysis shows that mutants lacking Tid1 form four-viable-spore tetrads with levels of interhomolog crossover (CO) and noncrossover recombination similar to, or slightly greater than, those in wild type. Importantly, *tid1* mutants show a marked defect in crossover interference, a mechanism that distributes crossover events nonrandomly along chromosomes during meiosis. Previous work showed that *dmc1*Δ mutants are strongly defective in strand invasion and meiotic progression and that these defects can be partially suppressed by increasing the copy number of *RAD54*. Tetrad analysis is used to show that meiotic recombination in *RAD54*-suppressed *dmc1*Δ cells is similar to that in *tid1*; the frequency of COs and gene conversions is near normal, but crossover interference is defective. These results support the proposal that crossover interference acts at the strand invasion stage of recombination.

MOST recombination events in budding yeast are initiated by enzymatic formation of double-strand breaks (DSBs). The pair of DNA ends formed by DSBs is processed to form single-stranded DNA (ssDNA) tails. Relatives of bacterial RecA protein act as "recombinases." Recombinases assemble on ssDNA and promote invasion of ssDNA into the homologous DNA duplex. Two recombinases, Rad51 and Dmc1, provide strand invasion activity during meiosis (reviewed in Roeder 1997). Both Rad51 and Dmc1 promote formation of homologous hybrid molecules *in vitro* (Sung 1994; Passy *et al.* 1999; Hong *et al.* 2001) and *in vivo* (Bishop *et al.* 1992; Shinohara *et al.* 1992, 1997a; Schwacha and Kleckner 1997). In spite of this redundant function, cytological and genetic observations indicate that the two RecA homologs often cooperate during strand invasion (Bishop 1994; Schwacha and Kleckner 1997; Shinohara *et al.* 2000). Cytological observations also suggest that Rad51 and Dmc1 often assemble as side-by-side oligomers at sites of recombination (Shinohara *et al.* 2000). The functional benefit derived from coordinated assembly of Rad51 and Dmc1 is not understood. However, it is known that coordinated assembly of recombinase is promoted by the recombination accessory factor Tid1 (Shinohara *et al.* 2000). Tid1 also stimulates recombinase-dependent strand invasion *in vitro* (Petukhova *et al.* 2000; E. Hong, S. van Komen, P. Sung and D. K. Bishop, unpublished observations) and *in vivo* (Shinohara *et al.* 1997b). A yeast paralogue of Tid1, Rad54, displays closely related biochemical activities (Petukhova *et al.* 1998). Furthermore, genetic studies indicate that the functions of Tid1 and Rad54 are partially redundant (Klein 1997; Shinohara *et al.* 1997b).

Strand invasion forms stretches of heteroduplex DNA that connect the broken chromatid to an unbroken homologous chromatid. Heteroduplex-containing connections between chromatids are referred to as homologous joint molecules (JMs). JMs are eventually resolved to yield two types of recombinants, crossovers (COs) and noncrossovers (NCOs). COs play a critical role in meiosis that is not played by NCOs (reviewed in Roeder 1997; Zickler and Kleckner 1999). COs contribute to accurate segregation by forming the physical connections between homologous chromosome pairs needed for stable bipolar attachment of pairs to the meiosis I spindle.

COs are not randomly distributed along chromosomes. The distribution is such that the probability of COs occurring close to one another is lower than expected if CO events occurred independently of one another (Sturtevant 1915; Muller 1916). This phenomenon is known as crossover interference. In addi-

[1]*Present address:* Research Institute for Radiation Biology and Medicine, Hiroshima University, Hiroshima 734-8553, Japan.

[2]*Corresponding author:* Department of Radiation and Cellular Oncology, Cummings Life Science Center, 920 E. 58th St., Chicago, IL 60637. E-mail: dbishop@midway.uchicago.edu

tion, crossovers are distributed among chromosomes such that the probability that a chromosome will be bereft of COs is lower than would be the case if COs were distributed randomly (Jones 1987).

The mechanism that regulates CO distribution in meiosis is not understood although several models have been proposed to account for it. Because the mechanism of interference requires that the outcome of one recombination event be influenced by a second nearby event, it can be thought of as involving three types of functions. First, sensors of COs or pre-CO intermediates trigger a signal. Second, transducers relay the signal from the triggering event to the target event. Third, effectors act to ensure that target events form NCOs rather than COs. Most models for interference focus on the mechanism of signal transduction rather than the mechanism of triggering and effector function. One group of hypotheses for interference signaling (Egel 1978; Maguire 1988; King and Mortimer 1990; Sym and Roeder 1994; Kaback *et al.* 1999) invokes the synaptonemal complex (SC), the ribbon-like proteinaceous structure that assembles along paired homologs as recombination progresses (reviewed in Zickler and Kleckner 1999). Interference signals are proposed to initiate at sites of COs and to spread outward along the SC, acting to block CO formation in adjacent regions of synapsed bivalents. Another model maintains that signaling occurs by imposition of axial stress on meiotic bivalents and local relief of stress when an event becomes committed to become a CO. In this model, local relief of stress prevents nearby intermediates from becoming COs (Storlazzi *et al.* 1996; Zickler and Kleckner 1999). Finally, the "counting" model maintains that a fixed number of NCOs separate COs; this rule could be satisfied by formation of a cluster of recombination intermediates with only one member of each cluster designated to become a CO (Foss *et al.* 1993; F. Stahl, personal communication).

Several *Saccharomyces cerevisiae* genes have been shown to be important for crossover interference (Sym and Roeder 1994; Chua and Roeder 1997; Nakagawa and Ogawa 1999; Novak *et al.* 2001). These include *ZIP1*, encoding a component of the SC central region; *MER3*, encoding a meiosis-specific DNA helicase; *MSH4*, encoding a protein related to the *Escherichia coli* mismatch repair protein MutS; and *NDJ1/TAM1*, encoding a telomere-associated protein. Mutation in all but one of these interference genes reduces the frequency of CO recombinants roughly threefold, indicating that the functions of these genes are required to form normal levels of CO products in addition to regulating the distribution of these products. *NDJ1/TAM1* (Chua and Roeder 1997; Conrad *et al.* 1997) differs from the other interference genes in that mutation of the gene does not reduce CO frequency (Chua and Roeder 1997).

Because early DSB recombination models account for formation of CO and NCO recombinants as resulting from alternative modes of Holliday junction resolution (Holliday 1964; Szostak *et al.* 1983), the influence of the interference signal has been thought to effect recombination at this late stage. However, *zip1* and *mer3* mutations were found to delay the conversion of DSBs to recombination products (Storlazzi *et al.* 1996; Nakagawa and Ogawa 1999). This result led to the proposal that interference might act at, before, or during the strand invasion stage (Storlazzi *et al.* 1996).

Here we show that crossover interference is defective in *tid1*Δ mutant strains. We also show that the recombination that occurs in *dmc1*Δ strains overexpressing *RAD54* lacks interference. These results support the proposal that crossover interference involves regulation of the strand invasion step of recombination. We consider several explanations for the mechanistic relationship between strand invasion and crossover interference, including one in which the crossover interference signal acts to block invasion of one of the two ends created by a meiotic DSB.

MATERIALS AND METHODS

Strains and plasmids: The strains used in this study are listed in Table 1. S2921 (*MAT***a** *leu2::hisG can1*^{R} *URA3 HOM3 TRP2 lys2 ho::LYS2*; Sym and Roeder 1994) and MSY620 (*MAT*α *leu2::hisG CAN1 ura3 hom3-10 trp2 lys2 ho::LYS2*) are congenic to SK-1. The *tid1* mutation (*tid1::LEU2*) was backcrossed 11 times to the isogenic derivatives of SK-1. *HIS4::LEU2* is a synthetic recombination hotspot (Cao *et al.* 1990). The *HIS4* construct contains a copy of the *LEU2* gene inserted centromere proximal to the *HIS4* coding region and a copy of the *URA3* gene inserted 12 kb farther away from *HIS4*. The *dmc1::ARG4* allele was from DKB625 (Bishop *et al.* 1992). The *tid1::leu2::TRP1* allele was constructed by transformation of a *leu2::TRP1* fragment from pLT11 (Cross 1997) into a *tid1::LEU2* strain (MSY084; Shinohara *et al.* 1997b). The *leu2-eco* allele was created by filling in the *Eco*RI site of *LEU2* with the Klenow fragment followed by one-step gene replacement.

Plasmid YCp-*KanMX4-TID1* (pMS139) is a derivative of YCplac22 (Gietz and Sugino 1988), which carries a 3.5-kb *Bam*HI fragment containing the *TID1* gene from pBS-*RDH54* (Shinohara *et al.* 1997b) inserted at the *Bam*HI site and a 1.4-kb *Not*I fragment containing the *KANMX4* construct from pFA6a-KANMX4 (Wach *et al.* 1994) inserted at the *Sma*I site. Plasmid YEp*RAD54* (pMS182) was constructed by inserting a *Pst*I-*Eco*RI fragment containing the wild-type *RAD54* gene into the *Pst*I-*Eco*RI site of pRS424 (YEp-*TRP1*$^+$; Christianson *et al.* 1992).

Genetic analysis: Previously described genetic procedures and media were used (Bishop *et al.* 1992). For tetrad analysis, parental haploid strains were mated for 6 hr on YPD plates and transferred onto sporulation (SPM) plates. After 24 hr incubation, the spores were dissected and incubated for 2 days prior to phenotyping by replica plating to SD medium containing appropriate combinations of amino acids. To minimize the possibility of dissection of false tetrads, digestion of asci was carried out on dissection plates by adding zymolyase immediately before streaking out ascus suspensions.

For analysis of interference and map distances, all tetrads showing non-Mendelian segregation of any markers were excluded from analysis. Interference values are expressed as the ratio of nonparental ditypes (NPDs) observed (NPD_{ob}) to NPDs expected (NPD_{ex}). The fraction of tetrads expected to be NPDs was determined from the Papazian equation: $NPD_{ex} = \frac{1}{2}[1 - T - (1 - 3T/2)^{2/3}]$ (Papazian 1952), where T is the

TABLE 1

Strains

Strain	Genotype	Reference
S2921	*MAT***a** *leu2::hisG can1*^{R} *URA3 HOM3 TRP2 lys2 ho::LYS2*	Sym and Roeder (1994)
NKY1543	*MAT*α *ho::LYS2 ura3 leu2::hisG lys2 his4X-LEU2-Bam*HI-*URA3 arg4-nsp*	Storlazzi *et al.* (1996)
MSY620	*MAT*α *leu2::hisG CAN1 ura3 hom3-10 trp2 lys2 ho::LYS2*	This study
MSY622	Derivative of S2921 with *tid1::LEU2*	This study
MSY626	Derivative of MSY620 with *tid1::LEU2*	This study
MSY818	Derivative of MSY622 with pMS139	This study
MSY835	*MAT*α *ho::LYS2, ura3, leu2::hisG, lys2, his4X-LEU2-Bam*HI-*URA3, arg4-nsp, trp1::hisG*	This study
MSY943	*MAT***a** *ho::LYS2 ura3 leu2::hisG lys2 his4B-leu2-eco arg4-bgl trp1::hisG*	This study
MSY962	Derivative of MSY943 with *tid1::leu2::TRP1*	This study
MSY964	Derivative of MSY835 with *tid1::leu2::TRP1*	This study
MSY1068	Derivative of MSY835 with *dmc1::ARG4*	This study
MSY1070	Derivative of MSY943 with *dmc1::ARG4*	This study
MSY1072	Derivative of MSY943 with *dmc1::ARG4* with pMS182	This study
MSY1153	*MAT***a** *ho::LYS2 ura3 leu2::hisG lys2 his4B-leu2-eco arg4-bgl*	This study
MSY1167	*MAT*α *ho::LYS2 ura3 leu2::hisG lys2 his4X-LEU2-Bam*HI-*URA3 trp1::hisG*	This study
MSY1172	*MAT*α *CAN1 ura3 hom3-10 trp2 lys2 ho::LYS2*	This study
MSY1174	*MAT***a** *can1*^{R} *URA3 HOM3 TRP2 lys2 ho::LYS2*	This study
MSY1176	*MAT***a** *ho::LYS2 ura3 leu2::hisG lys2 his4B-leu2-eco trp1::hisG*	This study
MSY1178	Derivative of MSY1176 with pMS182	This study
NKY1551	*MAT***a**/α *ho::LYS2/″ ura3/″ leu2::hisG/″ lys2/″ his4X-LEU2-Bam*HI-*URA3/his4B-LEU2 arg4-nsp/arg4-bgl*	This study
MSY134	Derivative of NKY1551 with *tid1::LEU2/″*	Shinohara *et al.* (1997b)

proportion of tetratypes observed. Data sets were analyzed using the χ^2 and χ^2 coincidence tests. To measure coincident double crossover in adjacent intervals, frequencies of tetrads with recombination in each of the two intervals are determined by summing *T*'s and NPDs for that interval and dividing by total tetrads. The expected frequency of coincident recombination is given by the product of the two single-interval frequencies (Chua and Roeder 1997). Map distances were determined using the standard mapping equation [cM = 100/2(T + 6 NPD)/(PD + T + NPD)] (Perkins 1949).

Tetrads showing 3:1 segregation of more than one marker or 4:0 segregation of at least one marker were presumed false and deleted from the data set prior to calculation of map distances and interference values. The method described in the appendix was used to estimate the contribution of false tetrads to the percentage of 3:1 tetrads. This allowed estimation of the "true" conversion frequency by subtracting the frequency estimated to have resulted from false tetrads from the observed frequency.

Cytology: Spread nuclei were stained with anti-Zip1 antibody (a generous gift from Dr. G. S. Roeder) and examined as described previously (Bishop 1994). Cumulative curves were constructed from time course data by a published method (Padmore *et al.* 1991).

RESULTS

Experimental system: Crossover interference can be detected in *S. cerevisiae* by phenotypic analysis of tetrads following sporulation of appropriately marked diploid strains. For this purpose we employed two systems in the efficiently sporulating SK-1 strain background. In the first system, a set of isogenic strains that contain a copy of chromosome *III* with four heterozygous markers, three of which are located in the vicinity of a strong recombination hotspot at the *HIS4* locus, was constructed (*HIS4::LEU2*, Figure 1, A and B; Cao *et al.* 1990). This hotspot was created by insertion of a copy of the *LEU2* gene downstream of *HIS4*. The second system for examining interference, which has been used extensively in previous studies (Sym and Roeder 1994), employs closely related congenic strains that carry heterozygosities at four well-separated sites on chromosome *V*. In both strains, haploid phenotypes from tetrads yielding four viable spores may be used to measure the strength of crossover interference. Four-viable-spore tetrads also allow the frequency of crossover recombination and non-Mendelian segregation (gene conversion) to be measured.

It was possible to examine the effect of a *tid1* null mutation on these three aspects of recombination without further modification of strains because homozygous *tid1* mutant diploid cells produce tetrad asci, and 58% of these asci contain four viable spores (Figure 1C). It is not possible to determine the effect of a *dmc1* null mutation in SK-1-derived strains without modification of the mutant strain because the mutation causes failure to repair meiotic DSB recombination intermediates and arrest in meiotic prophase via induction of a checkpoint control pathway. It is possible to suppress the DSB repair and sporulation defects of *dmc1*Δ mutations by introduction of a high-copy-number plasmid that carries the *RAD54* gene (YEp*RAD54*; Bishop *et al.* 1999). While our previous work yielded relatively modest levels of spore viability in *dmc1*Δ-YEp*RAD54* strains, the use of a different 2μ plasmid vector improved the level of spore viabil-

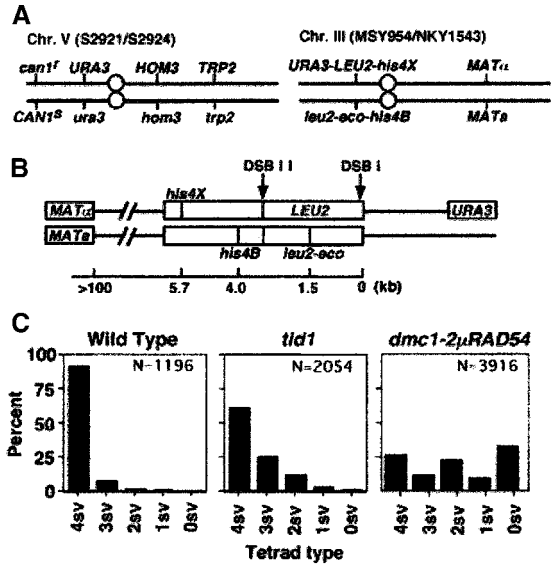

FIGURE 1.—Features of the experimental system. (A) The structure of chromosomes used for tetrad analysis of recombination. (B) The structure of the *HIS4::LEU2* recombination hotspot on chromosome *III*. The hotspot contains two strong DSB sites indicated as DSB I and DSB II. A more detailed description of the *HIS4::LEU2* region of chromosome *III* has been published (CAO *et al.* 1990; XU and KLECKNER 1995). The *leu2-eco* allele was created for this study by "filling in" the *Eco*RI site in *LEU2*. The distance of each marker from DSB I is shown. (C) Distribution of viable spores per ascus of *tid1* and *dmc1*Δ-YEp*RAD54*. *N*, number of tetrads examined.

ity to 50% with 23% of asci having four viable spores (Figure 1C). The viability pattern among *dmc1*Δ-YEp*RAD54* tetrads differs from that observed among *tid1* tetrads. In *dmc1*Δ-YEp*RAD54*, tetrads with two viable spores outnumbered those with three viable spores, suggesting that meiosis I nondisjunction is a major factor underlying the low viability of meiotic products. In *tid1*, the pattern of viability is that expected if occasional failure to resolve lethal recombination intermediates limits the viability of meiotic products. The relatively high spore viability promoted by the new YEp*RAD54* plasmid (pMS182) made tetrad analysis in a *dmc1*Δ/*dmc1*Δ strain feasible. To distinguish effects of the *dmc1*Δ mutation from those caused by the YEp*RAD54* plasmid, an isogenic *DMC1/DMC1* strain carrying the YEp*RAD54* plasmid was examined in parallel.

Interference can be detected for an interval defined by two linked markers by the ratio of the three different types of tetrads, parental ditypes (PDs), tetratypes (T's), and NPDs. NPD tetrads can arise only via two reciprocal crossover events involving all chromatids present at the time of meiotic recombination. This class is therefore diagnostic for double crossover (DCO) events in a given interval. Tetratypes often arise via single COs, but can also arise from DCOs that involve only three of the four chromatids present at the time of recombination. The expected frequency of NPDs can be calculated from the observed frequency of T's (PAPAZIAN 1952). Crossover interference is detected if the observed number of NPDs is significantly less than the number expected. Interference can also be measured by a method that looks at the segregation of three linked markers (CHUA and ROEDER 1997). In this method the number of coincident crossovers in two adjacent intervals is determined and compared to the number predicted on the basis of the assumption that crossover events are independent of one another. Evidence for interference is obtained if the observed amount of coincident COs is significantly less than the predicted amount. The ratio of observed to expected coincident COs is closely related to the so-called "coefficient of coincidence," which is used to measure interference in organisms that do not allow tetrad analysis (MULLER 1916; SNOW 1974).

Interference is defective in *tid1* and *dmc1*Δ-YEp*RAD54* strains: Tetrads from wild-type (*i.e.*, *DMC1 TID1*) strains were examined for crossover interference by calculation of the ratio of NPD_{ob}/NPD_{exp}. The values obtained were between 0.18 and 0.5 in agreement with previously published results for these markers (Table 2; SYM *et al.* 1993; NAKAGAWA and OGAWA 1999; NOVAK *et al.* 2001). The results also indicate that interference can be detected in the intervals adjacent to the *HIS4::LEU2* hotspot on chromosome *III* as shown previously (CAO *et al.* 1990). Interference was significantly reduced in *tid1* relative to *TID1*$^+$ for all marked intervals tested on chromosomes *V* and *III* ($P < 0.05$, Table 2). No crossover interference was detected in three of the six intervals and interference was significantly reduced in the remaining three intervals. A functional copy of *TID1* on a centromere-containing plasmid rescued the interference defect of the *tid1* mutant strain, indicating that *tid1* and not a hidden genetic difference between the congenic *tid1* and *TID1*$^+$ strains is responsible for the interference defect.

Interference was also examined in a *dmc1*Δ-YEp*RAD54* strain carrying markers on chromosome *III* (see Table 2). No interference was detected for the three marked intervals examined: the ratio of NPD_{ob} to NPD_{exp} is close to 1 in all three cases. The YEp*RAD54* plasmid was not responsible for the loss of interference observed in the *dmc1*Δ-YEp*RAD54* strain; wild-type levels of interference were seen in a *DMC1*-YEp*RAD54* control strain.

Data from strains carrying heterozygosities in chromosome *III* were also analyzed by the three-factor cross method (Table 3). Interference was readily detected as a significant difference between observed and expected frequencies of adjacent COs in the two *TID1 DMC1* control strains, but not in the *tid1* or *dmc1*Δ-YEp*RAD54* mutant strain. Together the results of tetrad analysis indicate that both the *tid1* and the *dmc1*Δ-YEp*RAD54* strains are defective in crossover interference.

***tid1* and *dmc1*Δ-YEp*RAD54* strains produce tetrads with near-normal numbers of interhomolog recombinants:** The frequency of COs can be measured using

TABLE 2

Crossover frequency and crossover interference

Strain[a]	Interval[b]	No. PD	No. T	No. NPD	Total[c]	Map distance[d]	Fold increase[e]	NPD_{ob}/NPD_{ex} (P)[f]	Deviation from wild type[g]
				Chromosome *V*					
TID1	*CAN1-URA3*	409	923	34	1366	41	—	0.19 (<0.0001)	—
	URA3-HOM3	455	859	52	1366	43	—	0.34 (<0.0001)	—
	HOM3-TRP2	1094	268	4	1366	11	—	0.50 (0.16)	—
tid1	*CAN1-URA3*	361	628	38	1027	42	1.0	0.37 (<0.0001)	0.01
	URA3-HOM3	363	608	56	1027	46	1.1	0.63 (0.0003)	0.007
	HOM3-TRP2	617	386	24	1027	26	2.4*	0.96 (0.84)	<0.0001
tid1-pTID1	*CAN1-URA3*	331	797	47	1175	46	0.9	0.32 (<0.0001)	0.001
	URA3-HOM3	320	804	51	1175	47	0.9	0.38 (<0.0001)	0.35
	HOM3-TRP2	828	342	5	1175	16	0.7	0.31 (0.006)	0.39
				Chromosome *III*					
TID1	*URA3-LEU2*	813	316	2	1131	14	—	0.14 (0.0013)	—
	LEU2-MAT	509	594	28	1131	34	—	0.42 (<0.0001)	—
	URA3-MAT	346	728	57	1131	47	—	0.40 (<0.0001)	—
tid1	*URA3-LEU2*	1002	186	5	1193	9.1	0.65	1.25 (0.62)	0.045
	LEU2-MAT	462	670	61	1193	43	1.3	0.70 (0.005)	<0.0001
	URA3-MAT	425	681	87	1193	50	1.1	0.95 (0.60)	0.0005
DMC1-YEp*RAD54*	*URA3-LEU2*	919	276	3	1198	12	—	0.33 (0.046)	—
	LEU2-MAT	529	641	28	1198	34	—	0.37 (<0.0001)	—
	URA3-MAT	379	772	47	1198	44	—	0.31 (<0.0001)	—
*dmc1*Δ-YEp*RAD54*	*URA3-LEU2*	1038	197	4	1239	8.9	0.74	1.0 (1.0)	0.61
	LEU2-MAT	599	581	59	1239	38	1.1	1.1 (0.41)	<0.0001
	URA3-MAT	542	617	80	1239	44	1.0	1.3 (0.03)	<0.0001

[a] Strains used were as follows. Chromosome *V*: *TID1*, MSY1172 × MSY1174; *tid1*, MSY622 × MSY626; *tid1-YCpTID1*, MSY626 × MSY818. Chromosome *III*: *TID1*, NKY1543 × MSY1153; *tid1*, MSY962 × MSY964; *DMC1*-YEp*RAD54*, MSY1176 × MSY1178; *dmc1*Δ-YEp*RAD54*, MSY1068 × MSY1072. *TID1* and *DMC1*-YEp*RAD54* controls carry the same number of functional copies of the amino acid biosynthetic gene used to mark the *tid1* and *dmc1* deletion alleles as do strains carrying the deletion alleles (*e.g.*, if the mutant strain is *tid1*Δ*::LEU2/tid1*Δ*::LEU2 leu2/leu2*, the wild-type control is *TID1/TID1 LEU2/LEU2*). Controls were designed in this way because previous work showed amino acid auxotrophy can alter gene conversion frequency (Abdullah and Borts 2001). Additional control experiments showed that absence of the amino acid biosynthetic genes used as markers in this study altered conversion frequency slightly, but did not substantially alter crossover frequency or crossover interference (data not shown).

[b] For chromosome *V*, *URA3* refers to the normal *URA3* locus. For chromosome *III URA3* and *LEU2* refer to insertions of those genes at the *HIS4* locus (see Figure 1).

[c] Only four-spore-viable tetrads that did not show non-Mendelian segregation were included.

[d] See materials and methods for method of calculation. Only four-spore-viable tetrads that did not show non-Mendelian segregation were used to calculate map distances.

[e] Ratio of map distance for mutant over wild-type control. Asterisk indicates significant differences between mutant and wild type.

[f] The fraction of NPDs expected (see materials and methods) divided by the fraction of NPDs observed. *P* values in parentheses indicate significant differences between NPD_{ob} and NPD_{ex}.

[g] *P* values indicating significance of differences between PD, T, and NPD frequencies between mutants and isogenic wild-type controls.

the standard genetic mapping equation (Perkins 1949). This equation takes into account the fact that a fraction of PD and T tetrads result from double COs and thereby gives an accurate estimate of the number of crossovers in a given interval. This method was used to determine the frequency of COs for three marked intervals on chromosome *III* in isogenic wild-type, *tid1*, and *dmc1*Δ-YEp*RAD54* strains (see Table 2). Three of the six intervals examined in *tid1* strains showed no significant difference with *TID1* controls while the remaining three intervals showed only modest differences; the *HOM3-TRP2* and *LEU2-MAT* intervals showed 2.3- and 1.3-fold increases in map distance, respectively, while the *URA3-LEU2* interval showed a 1.5-fold decrease ($P < 0.01$). In the case of *dmc1*Δ-YEp*RAD54*, map distances were not significantly different from those in the control strain for *LEU2-MAT* and *URA-MAT* while the *URA3-LEU2* interval was 1.3-fold longer ($P = 0.01$). Overall the mutants examined displayed very modest alterations in CO frequency for some intervals and no significant changes in others.

The frequency of 3:1 and 1:3 segregation of markers

TABLE 3

Analysis of coincident crossovers in adjacent intervals

Strain[a]	Total tetrads	Single intervals[b]		Adjacent intervals		Observed/expected	*P* value[e]
		URA3-LEU2	*LEU2-MAT*	Observed[c]	Expected[d]		
TID1	1141	0.278	0.543	0.106	0.151	0.70	0.0001
tid1	1201	0.156	0.609	0.096	0.095	1.01	0.85
DMC1-YEp*RAD54*	1208	0.228	0.559	0.081	0.127	0.64	<0.00001
*dmc1*Δ-YEp*RAD54*	1249	0.158	0.510	0.087	0.081	1.07	0.37

[a] See column 1 of Table 1 for names of strains used.
[b] Frequency of T plus NPD tetrads for interval indicated.
[c] Observed frequency of tetrads that are either T or NPD for both the *URA3-LEU2* and the *LEU2-MAT* intervals.
[d] "Expected" is the product of the frequencies given for the *URA3-LEU2* interval and the *LEU2-MAT* interval.
[e] *P* values reflect the likelihood that the difference between the expected and observed frequencies is attributable to chance as determined by a χ^2 test.

(gene conversion or non-Mendelian segregation) was estimated in the same data set used to analyze reciprocal crossovers (Table 4). Obtaining these estimates involved correction for the contribution of false tetrads to the observed number of 3:1 tetrads (see the APPENDIX for a description of the method used to make this correction). In the case of the *tid1* chromosome *V* experiment, data obtained from the two *TID1*$^+$ control strains were found to be statistically indistinguishable from one another. These two data sets were therefore combined before comparison to data from the *tid1* mutant strain. The frequency of 3:1 tetrads was about twofold higher in *tid1* compared to the combined *TID1*$^+$ control for both *CAN1* and *TRP2* and these differences were significant on the basis of Fisher's exact test ($P < 0.05$). The *tid1* mutant also showed higher 3:1 frequency for

TABLE 4

Frequencies of 3:1 segregation

Strain[a]	Total tetrads[b]	Predicted % of undiagnosed false tetrads	% 3:1 segregation[c]			
			CAN1	*URA3*	*HOM3*	*TRP2*
		Chromosome *V*				
TID1	1409	0.8	0.8/0.7	0.3/0.2	0.6/0.5	1.4/1.3
tid1-pTID1	1222	0.4	1.1/1.0	0.6/0.5	0.6/0.6	1.6/1.5
TID1 combined	2631	0.6	0.9/0.8	0.4/0.3	0.6/0.5	1.5/1.4
tid1	1118	2.9	2.4/1.8*	1.4/0.8	1.1/0.8	3.2/2.8*

Strain[a]	Total tetrads[b]	Predicted % of undiagnosed false tetrads	% 3:1 segregation[c]		
			MAT	*LEU2*	*URA3*
		Chromosome *III*			
TID1	1250	3.1	1.3/0.2[d]	6.4/6.2	1.8/1.5
tid1	1320	1.7	1.8/1.2*	6.4/6.2	1.5/1.3
DMC1-YEp*RAD54*	1275	0.4	0.7/0.5	4.5/4.5	0.9/0.8
*dmc1*Δ-YEp*RAD54*	1362	0.6	0.4/0.2	7.6/7.5*	0.7/0.6

Postmeiotic segregation was not detected in this experiment. Numbers presented are sums of the frequencies of $3^+:1^-$ and $1^+:3^-$ tetrads.
[a] See footnotes *a* and *b* of Table 2 for names of strains used and marker locations.
[b] Number of tetrads dissected minus the number of tetrads that were diagnostically false. The predicted percentage of undiagnosed false tetrads was calculated as $[(N_{F2} + N_{N3}) - (N_{m3:1} + N_{N4:0})]/\text{Total} \times 100$ (see APPENDIX).
[c] Percentages of observed frequencies/percentages corrected for the contribution of false tetrads (see APPENDIX) are shown. *, the corrected value of 3:1 frequency for a mutant is significantly different from that of the wild-type control on the basis of Fisher's exact test.
[d] The large correction factor required makes this value less reliable than other estimates (see text).

the *URA3* locus on chromosome *V*, but this difference was not significant once the contribution of false tetrads was taken into account, nor was the difference at the *HOM3* locus significant (with or without correction for false tetrads). With respect to chromosome *III* markers, mutation of *tid1* did not significantly alter conversion frequency of the hotspot proximal markers, *LEU2* and *URA3*. Correction of the data for the contribution of false tetrads suggested that mutation of *tid1* significantly increased conversion frequency at *MAT* from 0.2 to 1.2%. However, the large correction factor required to estimate *MAT* conversion frequency in the chromosome *III*-marked *TID1*$^+$ strain makes this measurement less reliable than others (see the APPENDIX for further discussion).

Comparison of data from the *dmc1*Δ-YEp*RAD54* strain with data from the *DMC1*-YEp*RAD54* control revealed a modest hyperconversion effect at *LEU2* (1.7-fold), but no significant difference in 3:1 frequency was detected at *URA3* or *MAT*. Thus for both *tid1* and *dmc1*Δ-YEp *RAD54*, some markers showed modest increases in conversion frequency relative to wild type while others were unaffected.

The hyperconversion effects could result from an increase in the average length of conversion tracts, an increase in the number of conversion events, or an increase in the use of homologs over sisters as recombination partners. The increase in conversion tract lengths seems most likely in light of the fact that DSBs undergo more extensive ssDNA resection in *tid1* than in wild type (SHINOHARA *et al.* 1997b). Owing to inefficient suppression of the *dmc1* block in the liquid medium required to achieve synchronous induction of DSBs, the amount of resection in *dmc1*Δ-YEp*RAD54* strains was not measured.

The *tid1* mutant accumulates Zip1-containing structures with normal appearance: Mutation of *dmc1* was previously shown to cause a defect in SC assembly (BISHOP *et al.* 1992; ROCKMILL *et al.* 1995). It was therefore of interest to determine if the *tid1* mutant is defective in SC assembly as well. Zip1 is a structural component of the SC central region (SYM *et al.* 1993). Immunostaining meiotic chromosome spreads for Zip1 protein can provide evidence for defects in synapsis. When viewed by fluorescence microscopy, Zip1 forms punctate structures that then elongate as chromosomes synapse. Zip1 and SCs then disappear at the end of prophase as CO recombination is completed and cells prepare to undergo the first meiotic division. Several mutants that are defective in synapsis accumulate a single large brightly staining Zip1 structure, the polycomplex (BISHOP *et al.* 1992; ROCKMILL *et al.* 1995; SYM and ROEDER 1995; CHUA and ROEDER 1997; NOVAK *et al.* 2001). To determine if *TID1* is required for normal synapsis, chromosome spreads of *TID1*$^+$ and *tid1* cells were indirectly immunostained for Zip1 protein (Figure 2). At 3 hr, the fraction of cells containing predominantly elongated Zip1 structures (Figure 2, category 3) was lower for the *tid1* mutant than for the *TID1*$^+$ control. In addition, the fraction of nuclei containing polycomplex was about threefold greater in *tid1* than in *TID1*$^+$. At 5 hr in meiosis, a large fraction of *tid1* nuclei had elongated Zip1 structures that appeared identical to those formed in wild type. The frequency of nuclei containing predominantly elongated Zip1 structures reached a peak of ~50% at 5 hr in *tid1* as compared to a peak of 15% at 3 hr in *TID1*$^+$. Time course data can be used to construct cumulative curves that define the time when cells in a culture enter or exit a stage of interest (Figure 2D; PADMORE *et al.* 1991). Application of this method indicates that while *tid1* mutant cells initiated Zip1 assembly at the same time as wild type, entry into the category 3 stage was delayed ~1 hr. In addition, exit from the category 3 stage was delayed 3 hr in *tid1* relative to wild type. Thus, the *tid1* mutant showed a modest delay in elongation of Zip1 structures and a more pronounced delay in Zip1 disappearance.

DISCUSSION

Analysis of map distances and gene conversion frequencies in *tid1* and *dmc1*Δ-YEp*RAD54* strains indicates that interference can be disrupted without a substantial change in CO frequency or in the ratio of COs to NCOs. A previous study of the *ndj1/tam1* mutant also showed reduced interference without a reduction in COs (CHUA and ROEDER 1997). Because crossover interference suppresses crossovers, a mutation that specifically eliminates crossover interference is expected to elevate CO frequency unless some interference-independent process limits the total number of COs. Identification of two mutants that have near-normal levels of COs but reduced CO interference suggests that the total number of COs that occur in budding yeast is limited by an interference-independent mechanism. The results with the *ndj1* group of interference mutants (*ndj1*, *tid1*, and *dmc1*Δ-YEp*RAD54*) are in marked contrast to results obtained with the *zip1* group of interference mutants (*zip1*, *mer3*, and *msh4*; SYM and ROEDER 1994; NAKAGAWA and OGAWA 1999; NOVAK *et al.* 2001). These mutants show roughly two- to threefold reductions in CO frequency with compensatory increases in NCOs, indicating that these genes promote formation of crossover recombinants in addition to promoting interference. The interference defects in *ndj1/tam1* (CHUA and ROEDER 1997), *tid1*, and *dmc1*Δ-YEp*RAD54* strains are more specific than those of the *zip1* group in that CO frequency is closer to normal.

The use of mutant analysis to determine the *in vivo* function of recombination proteins is often complicated by the possibility that the mechanism that forms recombinants in a particular mutant may differ in multiple aspects from the mechanism that forms recombinants in wild type. In such cases, a specific difference between

the properties of recombination in wild type and mutant may reflect only indirectly the function of the gene in question. Given that interhomolog recombination is quite efficient (although slightly delayed) in the *tid1* mutant, there is little reason to suppose that the recombination mechanism operating in the mutant differs dramatically from that in wild type (except that Tid1 does not contribute to the process). However, suppression of *dmc1* by YEp*RAD54* could activate a pathway that is quite different from the normal *DMC1*-dependent process. While this caveat should be kept in mind, we argue that it is quite likely that the mechanism underlying the interference defect in *tid1* mutants is related to that underlying the defect in *dmc1*Δ-YEp*RAD54*. This is because Tid1 is a functional partner of Dmc1 and because Tid1, Dmc1, and Rad54 are all known to promote strand invasion. In the discussion that follows we examine the significance of a functional connection between homologous strand invasion and CO interference. The *tid1* mutant data are viewed as the primary evidence for this connection and the *dmc1*Δ-YEp*RAD54* data are viewed as providing secondary support.

Possible interactions between strand invasion and interference: The mechanism through which strand exchange functions contribute to crossover interference remains to be determined. Genetic and biochemical data indicate both Dmc1 and Tid1 act directly at sites of recombination by promoting the strand invasion stage of recombination (Bishop *et al.* 1992; Bishop 1994; Shinohara *et al.* 1997b, 2000; Passy *et al.* 1999). Therefore, it is likely that these two proteins contribute to the interference mechanism at sites of recombination either by influencing the generation of interference signals from CO events or by acting as effectors to alter target events to NCOs. These possibilities are considered in turn.

Assembly of the SC has been proposed to contribute to interference by providing a means for signaling along chromosomes. Evidence consistent with this view includes the fact that two species of fungi that do not undergo synapsis also lack interference (reviewed in Kohli and Bahler 1994; Roeder 1997). In addition, mutation of the yeast *ZIP1* gene, which encodes a structural component of the central regions of the SC, eliminates interference (Sym *et al.* 1993). Given that both *tid1* and *dmc1* mutants show delays in SC assembly (this study; Bishop *et al.* 1992; Sym *et al.* 1993; Rockmill *et al.* 1995), it is possible the interference defects described here are consequences of defective SC assembly. In this view the incorporation of Dmc1 and Tid1 at sites of

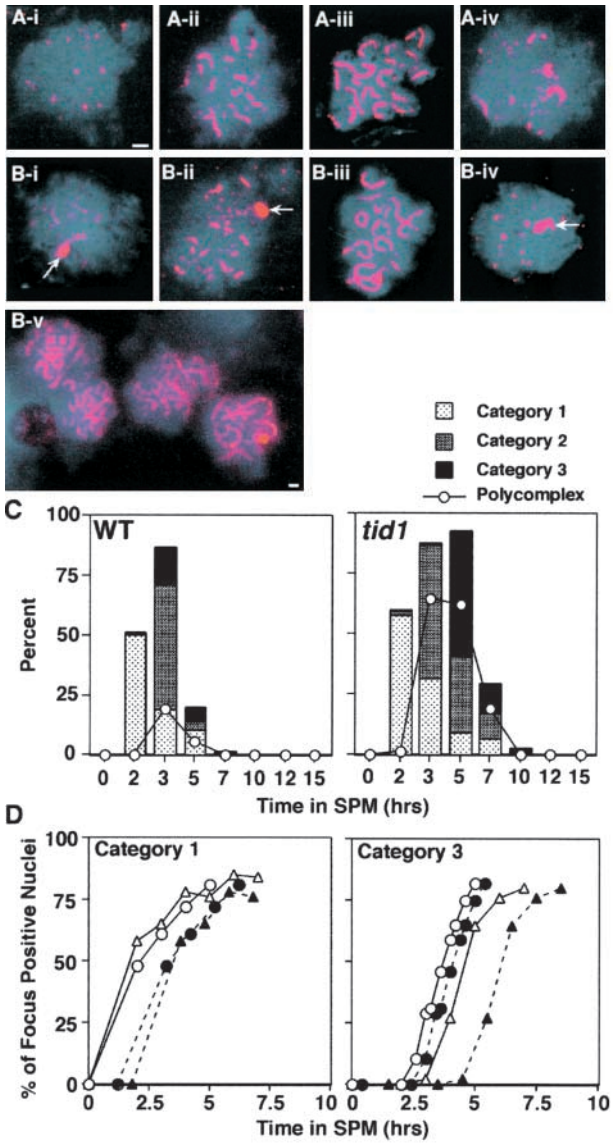

Figure 2.—Zip1 immunostaining. Meiotic cells were spread at indicated times and stained with anti-Zip1 antibody. The staining patterns were scored as belonging to one of three categories (Smith and Roeder 1997). Category 1 contains nuclei with only Zip1 foci, category 2 contains Zip1 foci together with partially elongated Zip1 structures, and category 3 contains predominantly elongated Zip1 structures. The time course was performed in strains (wild type, NKY1551; *tid1*, MSY134). (A and B) Representative nuclei. A-i to -iv, wild type: A-i, category 1 at 2 hr; A-ii, category 2 at 3 hr; A-iii, category 3 at 3 hr; A-iv, category 1 at 5 hr. B-i to -v, the *tid1* mutant: B-i, category 1 at 3 hr; B-ii, category 2 at 3 hr; B-iii, category 3 at 5 hr; B-iv, category 1 at 7 hr; B-v, category 3 nuclei at 5 hr (reduced magnification). Arrows indicate the polycomplexes of Zip1. Bars, 2 μm. (C) Time course analysis of Zip1-containing structures. Two hundred unselected nuclei were scored for SC structure and the presence or absence of a large brightly staining Zip1 structure (polycomplex) was noted. The percentage of each nucleus in each structural class is shown (bars) as well as the fraction of nuclei that contained polycomplex (open circles). (D) Cumulative curves constructed from the data shown in C (see materials and methods). Left, time of entry and exit from the stage at which category 1 nuclei are present (which is essentially equivalent to early zygotene); right, entry and exit from the category 3 stage (equivalent to pachytene). Open symbols, time of entry; closed symbols, time of exit; circles, *TID1*$^+$; triangles, *tid1*.

COs promotes efficient initiation of the SC, thereby promoting interference. However, this explanation seems unlikely at present because several observations suggest that synapsis is not necessary for interference. First, sites destined to give rise to COs can be distinguished cytologically from NCO sites because CO sites are associated with a specific structure, the late nodule (LN; reviewed by Zickler and Kleckner 1999). Studies in plants and fungi with favorable cytology suggest a one-to-one correspondence between LNs and COs and show that LNs are already present before significant synapsis occurs. Second, a *zip1* mutation alters the ratio of CO and NCO recombinants in a mutant strain background that is incapable of synapsis (Storlazzi *et al.* 1996), indicating that Zip1's role in controlling the CO/NCO decision may be independent of its role in forming the SC. Third, a recent study in Drosophila indicates that interference is normal in a mutant with a dramatic synapsis defect (Page and Hawley 2001). Finally, recent studies in yeast suggest that putative late nodule components are nonrandomly distributed in the absence of synapsis (G. S. Roeder, personal communication). Taken together these results challenge the notion that assembly of the SC central region is required for interference.

While the SC central region is unlikely to be required for interference, it is possible that the delays in synapsis seen in *dmc1* and *tid1* mutants are indirect consequences of defects in recombination-dependent chromosome structures. Such structural defects could, in turn, underlie the interference defects. For example, Zickler and Kleckner (1999) hypothesized that assembly of the Rad51-Dmc1 co-complex is asymmetric with respect to paired meiotic chromosome axes and that this asymmetry is important for development of interference signals.

TID1 and *DMC1* could also promote interference by acting as effectors of interference signals; *i.e.*, they may act to ensure that recombination events near COs give rise to NCOs. Recent findings are relevant to this possibility. First, invasion of one of the two ends created by meiotic DSBs often occurs well before invasion of the second end in wild-type cells (Hunter and Kleckner 2001). A second study showed that most or all double-Holliday junction (dHJ) intermediates detected by two-dimensional gel methods appear to be pre-COs because dHJs are resolved to COs after NCO products appear (Allers and Lichten 2001). NCOs may form without any second end invasion (Allers and Lichten 2001), perhaps by the mechanism known as synthesis-dependent strand annealing (see Figure 3 legend; Nassif *et al.* 1994; reviewed by Paques and Haber 1999). Together these results suggest that whether a recombination intermediate becomes a CO or a NCO may depend on whether or not the second end engages the single-end JM. The finding that the CO/NCO decision is likely to be associated with the activity of the second end, together with the finding that strand invasion functions

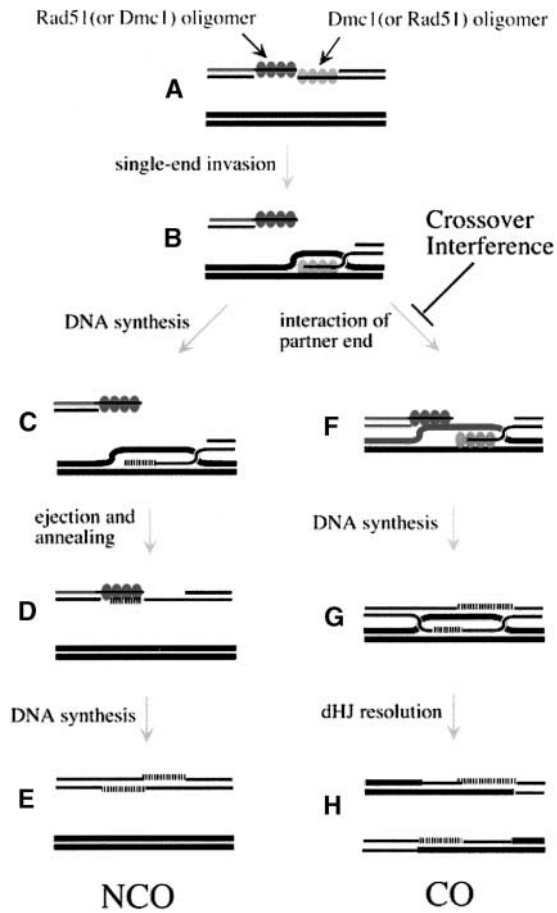

Figure 3.—Model for the impact of interference signals on strand invasion complexes. (A) The two ends at the site of a DSB are resected and different recombinase homo-oligomers are loaded on the two. (B) Strand invasion of one of the two ends occurs, forming a D-loop. The left branch of the pathway (C–E) shows events leading to NCOs. (C) Limited DNA synthesis from the 3′ of the invading end extends past the site corresponding to the location of the DSB. (D) The extended D-loop is ejected and newly synthesized sequences anneal to the partner end. (E) DNA repair synthesis and ligation form a NCO product. The right branch of the pathway (F–H) shows events leading to CO recombinants. (F) The D-loop is joined by invasion or annealing of the partner end. (G) DNA synthesis and ligation form a double-Holliday junction. (H) Holliday junction resolution forms a CO product. The model proposes that interference signals emanating from nearby CO events block the stable interaction of the partner end with the D-loop, thereby forcing resolution of the event via the NCO pathway.

are required for interference, leads us to a model for how interference signals alter recombination outcome. In this model, recombinase-mediated invasion of one of the two ends is blocked by the interference signal.

To account for specific inhibition of only one of two partner DNA ends, we propose that the sensitivity of one end to the interference signal depends on proper assembly of a Rad51-Dmc1 co-complex. On the basis of cytological observations, we previously hypothesized that the co-complex consists of a Rad51 homo-oligomer

on one DNA end and a Dmc1 homo-oligomer on the partner end (Figure 3; Shinohara *et al.* 2000). This arrangement has also been proposed on the basis of mutant effects on the accumulation of single-end JMs (unpublished observations cited in Hunter and Kleckner 2001). The notion of Dmc1 on one end and Rad51 on the other has additional appeal in the context of the model under consideration; it provides a means for the interference signal to specifically inactivate the invasion activity of one of the two ends. The Dmc1-ssDNA oligomer could be sensitive to the interference signal, while the Rad51-ssDNA oligomer is insensitive, or vice versa. Assembly of the same recombinase on a single pair of ends could render both ends insensitive to the interference signal or could block invasion completely until the interference signal dissipates. The finding that a *tid1* mutant shows a partial defect in side-by-side assembly of the two recombinases and a partial defect in interference is consistent with the model. The lack of interference in *dmc1*Δ-YEp*RAD54* could result from assembly of Rad51 on both ends created by a DSB.

Dmc1 regulation: In the SK-1 strain background used in this study, *DMC1* is strongly required for the conversion of DSBs to JMs (Bishop *et al.* 1992; Hunter and Kleckner 2001; Schwacha and Kleckner 1997). The requirement for *DMC1* for the strand invasion stage of recombination seems straightforward in light of the fact that Dmc1 protein promotes strand invasion *in vitro*. However, additional studies suggest that *dmc1* null mutant cells can efficiently repair meiotic DSBs under certain conditions. These conditions include cells overexpressing Rad54 (Bishop *et al.* 1999; this study), cells returned to mitotic growth medium (Bishop *et al.* 1992; Schwacha and Kleckner 1997; Shinohara *et al.* 1997a; Zenvirth *et al.* 1997), and cells carrying mutations in a gene required for synapsis, *RED1* (Schwacha and Kleckner 1997; Bishop *et al.* 1999). Studies in a different strain background (the "BR" background) suggest that DSB repair can occur even in *RED1*$^+$ *dmc1*Δ cells that are allowed to complete meiosis (Rockmill and Roeder 1994; Rockmill *et al.* 1995). Together, these results suggest that the strong block in progression from DSBs to JMs seen in SK-1 *dmc1* cells does not reflect limited strand invasion activity. Instead, there appears to be a regulatory constraint that blocks invasion in the absence of Dmc1. This study suggests that at least one function of this constraint is to ensure that Dmc1 is incorporated into recombination complexes so that CO distribution can be regulated.

Previous studies indicated that *DMC1* might regulate recombination events by promoting the choice of a homologous chromatid over a sister chromatid (Schwacha and Kleckner 1997). Mutation of *dmc1* altered recombination partner choice in favor of sister-sister interaction in *red1* cells and in meiotic cells returned to mitotic growth. A role in interhomolog partner choice could also explain modest recombination defects observed in *dmc1* mutant BR cells (Rockmill and Roeder 1994; Rockmill *et al.* 1995). In the present study, suppression of the *dmc1* block in the SK-1 strain background by high-copy numbers of *RAD54* resulted in normal or near-normal levels of interhomolog recombination among four-viable-spore tetrads.

There are several explanations for the finding that the frequency of interhomolog recombination is not reduced among four-viable-spore tetrads produced by *dmc1*Δ-YEp*RAD54* diploids. First, selection of tetrads with four viable spores may have resulted in selection of a subpopulation of cells that were particularly successful at negotiating the meiotic program in the absence of one of their recombination genes. Such selection could, in principle, obscure reductions in interhomolog recombination frequency in the total population of meiotic cells. Selection of four-viable-spore tetrads is somewhat unlikely to account for the failure to detect reductions in CO recombination in *tid1* and *dmc1*Δ-YEp*RAD54* mutants because such reductions have been detected for three other interference mutants (Sym and Roeder 1994; Nakagawa and Ogawa 1999; Novak *et al.* 2001). However, we cannot exclude the possibility of an ascertainment bias if the *dmc1*Δ-YEp*RAD54* cells partition into two subpopulations during meiosis, one being defective in completing interhomolog but not intersister recombination and a second that completes interhomolog recombination and goes on to form tetrads. A second possibility is that *DMC1* is needed for efficient interhomolog partner choice, but high copy numbers of *RAD54* substitute for this function. This explanation also seems unlikely in light of other observations suggesting that *RAD54* favors intersister, rather than interhomolog, recombination (Klein 1997; Arbel *et al.* 1999; Bishop *et al.* 1999). A third possibility is that *DMC1*'s role in promoting efficient interhomolog recombination is indirect; *i.e.*, *DMC1* may promote efficient progression on a pathway that leads to interhomolog recombination, but not selection of interhomolog donors *per se*. Thus, increasing *RAD54* copy number may bypass the block to progression on the *DMC1*-dependent path, thereby allowing normal partner choice functions to exert their influence. Finally, it is also possible that *DMC1* does play a direct role in homolog partner choice in wild-type cells, but in regions other than the chromosome *III* region examined here.

We thank Shirleen Roeder for generously providing strains and antibodies. We are grateful to John Game, Shelly Esposito, David Kaback, and Nancy Kleckner for helpful discussions. We also thank Anne Villeneuve for critical reading of an early version of this manuscript and Ted Karrison for advice on data analysis. This work was supported by NIGMS grant GM50936 to D.K.B.; by the Japanese Ministry of Education, Culture, Sports, Science, and Technology to A.S.; and by a Human Frontier Science Program grant to A.S. and D.K.B. M.S. was supported by postdoctoral and long-term fellowships from the Human Frontier Science Program.

LITERATURE CITED

Abdullah, M. F., and R. H. Borts, 2001 Meiotic recombination frequencies are affected by nutritional states in *Saccharomyces cerevisiae*. Proc. Natl. Acad. Sci. USA **98:** 14524–14529.

Allers, T., and M. Lichten, 2001 Differential timing and control of noncrossover and crossover recombination during meiosis. Cell **106:** 47–57.

Arbel, A., D. Zenvirth and G. Simchen, 1999 Sister chromatid-based DNA repair is mediated by *RAD54*, not by *DMC1* or *TID1*. EMBO J. **18:** 2648–2658.

Bishop, D. K., 1994 RecA homologs Dmc1 and Rad51 interact to form multiple nuclear complexes prior to meiotic chromosome synapsis. Cell **79:** 1081–1092.

Bishop, D. K., D. Park, L. Xu and N. Kleckner, 1992 *DMC1*: a meiosis-specific yeast homolog of *E. coli recA* required for recombination, synaptonemal complex formation, and cell cycle progression. Cell **69:** 439–456.

Bishop, D. K., Y. Nikolski, J. Oshiro, J. Chon, M. Shinohara *et al.*, 1999 High copy number suppression of the meiotic arrest caused by a *dmc1* mutation: *REC114* imposes an early recombination block and *RAD54* promotes a *DMC1*-independent DSB repair pathway. Genes Cells **4:** 425–444.

Cao, L., E. Alani and N. Kleckner, 1990 A pathway for generation and processing of double-strand breaks during meiotic recombination in *S. cerevisiae*. Cell **61:** 1089–1101.

Christianson, T. W., R. S. Sikorski, M. Dante, J. H. Shero and P. Hieter, 1992 Multifunctional yeast high-copy-number shuttle vectors. Gene **110:** 119–122.

Chua, P. R., and G. S. Roeder, 1997 Tam1, a telomere-associated meiotic protein, functions in chromosome synapsis and crossover interference. Genes Dev. **11:** 1786–1800.

Conrad, M. N., A. M. Dominguez and M. E. Dresser, 1997 Ndj1p, a meiotic telomere protein required for normal chromosome synapsis and segregation in yeast. Science **276:** 1252–1255.

Cross, F. R., 1997 'Marker swap' plasmids: convenient tools for budding yeast molecular genetics. Yeast **13:** 647–653.

Egel, R., 1978 Synaptonemal complex and crossing-over: Structural support or interference? Heredity **41:** 233–237.

Foss, E., R. Lande, F. W. Stahl and C. M. Steinberg, 1993 Chiasma interference as a function of genetic distance. Genetics **133:** 681–691.

Gietz, R. D., and A. Sugino, 1988 New yeast-*Escherichia coli* shuttle vectors constructed with in vitro mutagenized yeast genes lacking six-base pair restriction sites. Gene **74:** 527–534.

Holliday, R., 1964 A mechanism for gene conversion in fungi. Genet. Res. **5:** 282–304.

Hong, E. L., A. Shinohara and D. K. Bishop, 2001 *Saccharomyces cerevisiae* Dmc1 protein promotes renaturation of single-strand DNA (ssDNA) and assimilation of ssDNA into homologous supercoiled duplex DNA. J. Biol. Chem. **276:** 41906–41912.

Hunter, N., and N. Kleckner, 2001 The single-end invasion: an asymmetric intermediate at the double-strand break to double-Holliday junction transition of meiotic recombination. Cell **106:** 59–70.

Jones, G. H., 1987 Chiasmata, pp. 213–244 in *Meiosis*, edited by P. B. Moens. Academic Press, Orlando, FL.

Kaback, D. B., D. Barber, J. Mahon, J. Lamb and J. You, 1999 Chromosome size-dependent control of meiotic reciprocal recombination in *Saccharomyces cerevisiae:* the role of crossover interference. Genetics **152:** 1475–1486.

King, J. S., and R. K. Mortimer, 1990 A polymerization model of chiasma interference and corresponding computer simulation. Genetics **126:** 1127–1138.

Klein, H. L., 1997 *RDH54*, a *RAD54* homologue in *Saccharomyces cerevisiae*, is required for mitotic diploid-specific recombination and repair and for meiosis. Genetics **147:** 1533–1543.

Kohli, J., and J. Bahler, 1994 Homologous recombination in fission yeast: absence of crossover interference and synaptonemal complex. Experientia **50:** 295–306.

Maguire, M. P., 1988 Crossover site determination and interference. J. Theor. Biol. **134:** 565–570.

Muller, H. J., 1916 The mechanism of crossing over. Am. Nat. **50:** 193–221.

Nakagawa, T., and H. Ogawa, 1999 The *Saccharomyces cerevisiae MER3* gene, encoding a novel helicase-like protein, is required for crossover control in meiosis. EMBO J. **18:** 5714–5723.

Nassif, N., J. Penney, S. Pal, W. R. Engels and G. B. Gloor, 1994 Efficient copying of nonhomologous sequences from ectopic sites via P- element-induced gap repair. Mol. Cell. Biol. **14:** 1613–1625.

Novak, J. E., P. B. Ross-Macdonald and G. S. Roeder, 2001 The budding yeast Msh4 protein functions in chromosome synapsis and the regulation of crossover distribution. Genetics **158:** 1013–1025.

Padmore, R., L. Cao and N. Kleckner, 1991 Temporal comparison of recombination and synaptonemal complex formation during meiosis in *S. cerevisiae*. Cell **66:** 1239–1256.

Page, S. L., and R. S. Hawley, 2001 c(3)G encodes a *Drosophila* synaptonemal complex protein. Genes Dev. **15:** 3130–3143.

Papazian, H. P., 1952 The analysis of tetrad data. Genetics **37:** 175–189.

Paques, F., and J. E. Haber, 1999 Multiple pathways of recombination induced by double-strand breaks in *Saccharomyces cerevisiae*. Microbiol. Mol. Biol. Rev. **63:** 349–404.

Passy, S. I., X. Yu, Z. Li, C. M. Radding, J. Y. Masson *et al.*, 1999 Human Dmc1 protein binds DNA as an octameric ring. Proc. Natl. Acad. Sci. USA **96:** 10684–10688.

Perkins, D. D., 1949 Biochemical mutants in the smut fungus *Ustilago maydis*. Genetics **34:** 607–626.

Petukhova, G., S. Stratton and P. Sung, 1998 Catalysis of homologous DNA pairing by yeast Rad51 and Rad54 proteins. Nature **393:** 91–94.

Petukhova, G., P. Sung and H. Klein, 2000 Promotion of Rad51-dependent D-loop formation by yeast recombination factor Rdh54/Tid1. Genes Dev. **14:** 2206–2215.

Rockmill, B., and G. S. Roeder, 1994 The yeast *med1* mutant undergoes both meiotic homolog nondisjunction and precocious separation of sister chromatids. Genetics **136:** 65–74.

Rockmill, B., M. Sym, H. Scherthan and G. S. Roeder, 1995 Roles for two RecA homologs in promoting meiotic chromosome synapsis. Genes Dev. **9:** 2684–2695.

Roeder, G. S., 1997 Meiotic chromosomes: it takes two to tango. Genes Dev. **11:** 2600–2621.

Schwacha, A., and N. Kleckner, 1997 Interhomolog bias during meiotic recombination: meiotic functions promote a highly differentiated interhomolog-only pathway. Cell **90:** 1123–1135.

Shinohara, A., H. Ogawa and T. Ogawa, 1992 Rad51 protein involved in repair and recombination in *S. cerevisiae* is a RecA-like protein. Cell **69:** 457–470.

Shinohara, A., S. Gasior, T. Ogawa, N. Kleckner and D. K. Bishop, 1997a *Saccharomyces cerevisiae recA* homologues *RAD51* and *DMC1* have both distinct and overlapping roles in meiotic recombination. Genes Cells **2:** 615–629.

Shinohara, M., E. Shita-Yamaguchi, J. M. Buerstedde, H. Shinagawa, H. Ogawa *et al.*, 1997b Characterization of the roles of the *Saccharomyces cerevisiae RAD54* gene and a homologue of *RAD54*, *RDH54/TID1*, in mitosis and meiosis. Genetics **147:** 1545–1556.

Shinohara, M., S. L. Gasior, D. K. Bishop and A. Shinohara, 2000 Tid1/Rdh54 promotes colocalization of Rad51 and Dmc1 during meiotic recombination. Proc. Natl. Acad. Sci. USA **97:** 10814–10819.

Smith, A. V., and G. S. Roeder, 1997 The yeast Red1 protein localizes to the cores of meiotic chromosomes. J. Cell Biol. **136:** 957–967.

Snow, R., 1974 Maximum likelihood estimation of linkage and interference from tetrad data. Genetics **92:** 231–245.

Storlazzi, A., L. Xu, A. Schwacha and N. Kleckner, 1996 Synaptonemal complex (SC) component Zip1 plays a role in meiotic recombination independent of SC polymerization along the chromosomes. Proc. Natl. Acad. Sci. USA **93:** 9043–9048.

Sturtevant, A. H., 1915 The behavior of the chromosomes as studied through linkage. Z. Indukt. Abstammungs. Vererbungsl. **13:** 234–287.

Sung, P., 1994 Catalysis of ATP-dependent homologous DNA pairing and strand exchange by yeast Rad51 protein. Science **265:** 1241–1243.

Sym, M., and G. S. Roeder, 1994 Crossover interference is abolished

in the absence of a synaptonemal complex protein. Cell **79:** 283–292.

Sym, M., and G. S. Roeder, 1995 Zip1-induced changes in synaptonemal complex structure and polycomplex assembly. J. Cell Biol. **128:** 455–466.

Sym, M., J. A. Engebrecht and G. S. Roeder, 1993 ZIP1 is a synaptonemal complex protein required for meiotic chromosome synapsis. Cell **72:** 365–378.

Szostak, J. W., T. L. Orr-Weaver, R. J. Rothstein and F. W. Stahl, 1983 The double-strand-break repair model for recombination. Cell **33:** 25–35.

Wach, A., A. Brachat, R. Pohlmann and P. Philippsen, 1994 New heterologous modules for classical or PCR-based gene disruptions in *Saccharomyces cerevisiae*. Yeast **10:** 1793–1808.

Xu, L., and N. Kleckner, 1995 Sequence non-specific double-strand breaks and interhomolog interactions prior to double-strand break formation at a meiotic recombination hot spot in yeast. EMBO J. **14:** 5115–5128.

Zenvirth, D., J. Loidl, S. Klein, A. Arbel, R. Shemesh *et al.*, 1997 Switching yeast from meiosis to mitosis: double-strand break repair, recombination and synaptonemal complex. Genes Cells **2:** 487–498.

Zickler, D., and N. Kleckner, 1999 Meiotic chromosomes: integrating structure and function. Annu. Rev. Genet. **33:** 603–754.

Communicating editor: L. S. Symington

APPENDIX

We present the method used for estimating the contribution of false tetrads to the data presented above. The method employs the frequency of diagnostically false tetrads combined with the predicted distribution of false tetrad genotypes. It allows correction for the effect of false tetrads on gene conversion frequency estimates.

About 1.8% of the 9121 tetrads analyzed in this work were 4:0 for at least one marker or 3:1 for at least two markers. The two unusual tetrad classes are referred to as 4:0 tetrads and m3:1 tetrads, respectively. Tetrads showing 3:1 for a single marker are referred to as s3:1 tetrads. Analysis of heterozygous markers on different chromosomes showed a high degree of association between m3:1 on one chromosome and 3:1 of a marker on a second chromosome. This high association of non-Mendelian behavior of markers on different chromosomes is expected if spores from different asci associate, forming false tetrads prior to or during dissection. In the analysis below we assume that true coconversion of the markers used in the study occurs rarely if at all and we take m3:1 and 4:0 tetrads as diagnostically false.

Given that the frequency of diagnostically false tetrads was similar to expected gene conversion frequencies, it was of interest to determine the influence of false tetrads on calculated values of gene conversion frequency. We also wanted to show that false tetrads did not make a significant contribution to calculated map distances and interference values. For this purpose it was necessary to estimate the total number of false tetrads in the experimental data and the fraction of tetrads in certain key classes that were false. The classes of interest include s3:1 tetrads as well as PDs, T's, and NTPs for each marked interval. The genotype distribution among false tetrads was simulated by manipulating the experimental data set. This approach was facilitated by the use of Mactetrad (a "macro" program written for Microsoft Excel software). Mactetrad automates analysis of linkage and non-Mendelian segregation. Two simulations were performed for each *tid1* strain. The first simulation determined the array of genotypes produced by false tetrads containing two spores from one ascus and two from another (dyad-dyad false tetrads). The second simulation determined the distribution of genotypes produced by false tetrads containing three spores from one ascus plus a single spore from another ascus. The other two remaining types of false tetrads (dyad plus two monads and four monads) require association of spores from three different asci. These two types are expected to be quite rare and to contribute genotypes with a distribution very similar to that produced by dyad-dyad tetrads. We therefore use the dyad-dyad simulation to predict the distribution of all false tetrads containing no more than two spores from a single ascus. Such false tetrads are referred to hereafter as f2's. False tetrads containing three spores from the same ascus are referred to as f3's. The simulations were done by starting with a database file containing the tetrad genotype data from dissection of the strain of interest. The records of diagnostically false tetrads (4:0 and m3:1 tetrads) were deleted prior to carrying out the simulation. In each case, the f2 simulation was achieved by moving the records of the first two spores to the end of the file, thereby offsetting the genotype records by two. The f3 simulation was carried out in an equivalent manner, but with relocation of a single-spore genotype record. After rearranging the records in the manner described, the files were analyzed using the "Mark-non:2-2 Tetrads" and "Analyze Linkage" programs. The output of these programs was used to determine the fraction of simulated false tetrads displaying the various genotypes of interest.

We present the results of analysis of data from the *tid1* mutant strain M622/626 as an example. This data contained the highest percentage of diagnostically false tetrads of all strains examined (5.7%). The results of the two false tetrad simulations for M622/626 are summarized in Table A1. Note that for both the f2 and f3 simulations only ~70% of simulated false tetrads have genotypes that are diagnostic (*i.e.*, 4:0 or m3:1). The remaining tetrads either are s3:1 tetrads or show 2:2 for all four markers.

To estimate the relative contribution of the f2 and f3 types of false tetrads to the data set, we started with the frequency of 4:0 tetrads. This class is diagnostic for f2's as it occurs only in f3's in rare cases where the three spores from a true gene conversion triad contain the same allele and associate with a single spore from another tetrad that also contains the same allele. In contrast, m3:1 tetrads are frequent among both f2's and f3's. The total number of f2's in the sample (N_{f2}) was estimated by dividing the number of observed 4:0's

TABLE A1

Summary of false tetrad simulations using M622/626 data

Tetrad class	No. in data set	No. from f2 simulation	Frequency from f2 simulation	No. from f3 simulation	Frequency from f3 simulation
m3:1	60	558	0.50	737	0.66
4:0	8	214	0.19	5	<0.01
s3:1	91	260	0.23	248	0.22
2:2	1027	86	0.08	128	0.11
Total	1186	1118		1118	

($N_{4:0}$) by the fraction of f2's in the simulation that were 4:0's ($f_{\text{f2-4:0-sim}}$):

$$N_{\text{f2}} = N_{4:0}/f_{\text{f2-4:0-sim}} = 8/0.19 = 41.79.$$

With the number of f2's in hand, it is possible to determine the total number of f3's (N_{f3}) as follows. First, the number of m3:1 tetrads contributed by f2's ($N_{\text{f2-m3:1}}$) is determined. This number is given by the fraction of simulated f2's that are m3:1 ($f_{\text{f2-m3:1-sim}}$) multiplied by N_{f2}:

$$N_{\text{f3m3:1}} = N_{\text{f2}} \times f_{\text{f2-m3:1-sim}} = 41.79 \times 0.50 = 20.9.$$

The remaining m3:1 tetrads (60 − 20.9 = 39.1) are expected to be contributed by f3's ($N_{\text{f3-m3:1}}$). The data from the second simulation indicate that the fraction of f3's expected to be m3:1's ($f_{\text{f3m3:1-sim}}$) is 0.67. This number allows calculation of the total number of f3's:

$$N_{\text{f3}} = N_{\text{f3-m3:1}}/f_{\text{f3-m3:1-sim}} = 39.1/0.67 = 58.4.$$

In summary, the simulations indicate that ~42 tetrads in the data set are f2 tetrads and ~58 are f3 tetrads.

Having determined the total number of false tetrads in the sample, the simulated distribution can be used to determine the fraction of each tetrad class contributed by false tetrads. The number of false tetrads of a given type is multiplied by the fraction of false tetrads predicted to have a genotype of interest. For example, the number of single-site 3:1's for *CAN1* contributed by f2's ($N_{\text{f2-s3:1}CAN1}$) is given by

$$N_{\text{f2-s3:1}CAN1} = N_{\text{f2}} \times f_{\text{f2-s3:1}CAN1\text{-sim}} = 41.79 \times 0.07 = 2.92.$$

This type of calculation was done for all classes of interest and the numbers obtained for the contributions of f2's and f3's were added to give the estimated contribution of false tetrads to each class. The results for analysis of the contribution of false tetrads to PDs, T's, and NPDs are shown in Table A2. The results for single-site 3:1 segregation are shown in Table A3.

The analysis clearly indicates that false tetrads did not make a substantial contribution to the observed number of PDs, T's, and NPDs in the experimental data; they are predicted to represent <1.5% of tetrads in each class. This is also true for the other six data sets presented. In contrast, up to 42% of s3:1 tetrads in the MSY622/626 experiment are estimated to be false. To calculate corrected frequencies of gene conversion, the number of false s3:1 tetrads was subtracted from the total number of s3:1 tetrads in the experimental data.

TABLE A2

Contribution of false tetrads to PDs, T's, and NPDs in M622/626 data

Tetrad class	No. in data set (N = 1118)	Frequency from simulation		Estimated no. contributed to data set by false tetrads			% contributed by false tetrads
		f2	f3	f2	f3	f2 + f3	
CAN1-URA3							
PD	378	0.044	0.048	1.83	2.83	4.66	1.23
T	656	0.027	0.064	1.12	3.77	4.90	0.75
NPD	42	0.006	0.002	0.26	0.10	0.37	0.88
URA3-HOM3							
PD	389	0.033	0.047	1.38	2.78	4.16	1.07
T	642	0.037	0.064	1.53	3.77	5.31	0.83
NPD	59	0.007	0.003	0.30	0.16	0.46	0.78
HOM3-TRP2							
PD	648	0.061	0.074	2.54	4.35	6.89	1.06
T	398	0.014	0.038	0.60	2.25	2.85	0.72
NPD	24	0.002	0.002	0.07	0.10	0.18	0.75

TABLE A3

Contribution of false tetrads to single-site 3:1 tetrads in M622/626 data

Tetrad class	No. in data set (N = 1118)	Frequency from simulation		Estimated no. contributed to data set by false tetrads			% contributed by false tetrads
		f2	f3	f2	f3	f2 + f3	
CAN1	27	0.07	0.08	2.92	4.66	7.59	28
URA3	16	0.08	0.06	3.18	3.62	6.79	42
HOM3	12	0.04	0.03	1.79	1.94	3.73	31
TRP2	36	0.05	0.05	2.02	2.78	4.80	13

This method was used to generate the corrected conversion frequencies shown in Table 4.

The conversion frequency correction factors generated by this method were either modest or negligible (between 0.5 and 1.0) with an exception being *MAT* conversion in the chromosome *III*-marked *TID1*$^+$ strain. Because only three markers were followed in the chromosome *III* experiments, and because *MAT* is not closely linked to the other two markers, a large fraction of false tetrads (15% for f2's and 19% for f3's) from these strains are predicted to show 3:1 for *MAT* alone. This, combined with a relatively high frequency of false tetrads in the marked chromosome *III TID1*$^+$ experiment, resulted in a correction factor of 0.15. This means that the majority of s3:1 tetrads for *MAT* in this experiment were false, which makes the estimate of "true" conversions less reliable than estimates from other experiments. In contrast to the situation with *MAT*, the correction factors calculated for *LEU2* and *URA3* from the same data set are quite small, 0.97 and 0.83. This is because linkage of these markers is such that >90% of false tetrads showing 3:1 for one marker also show 3:1 for the other and are thereby directly recognized as false.

It should be noted that the method described above is applicable only if most 4:0 tetrads in a data set are false rather than being true tetrads that resulted from homozygosis of one or more markers prior to induction of sporulation. Homozygosis of markers can be a consequence of mitotic recombination or of meiotic recombination if a cell undergoes meiosis prematurely (during the growth of the culture) and resulting spores of like genotype mate. Premature meiosis can be a problem in the SK-1 strain background we use. In our experiments this problem was avoided by mating haploid parents shortly before transfer of diploid cells to sporulation medium as described in MATERIALS AND METHODS. A collection of false 4:0 tetrads can be distinguished from a collection of 4:0 tetrads resulting from homozygosis because the majority of the former will tend to display 3:1 of at least one other marker while the latter will not.